Published in final edited form as:
Curr Biol. 2019 October 07; 29(19): 3244–3255.e4. doi:10.1016/j.cub.2019.08.022.

Precise Coordination of Three-dimensional Rotational Kinematics by Ventral Tegmental Area GABAergic Neurons

Ryan N. Hughes[1], **Glenn D.R. Watson**[1], **Elijah A. Petter**[1], **Namsoo Kim**[1], **Konstantin I. Bakhurin**[1], **Henry H. Yin**[1,2]

[1]Department of Psychology and Neuroscience, Duke University, Durham, NC, 27708, USA.

[2]Department of Neurobiology, Duke University School of Medicine, Durham, NC, 27708, USA.

Summary

The Ventral Tegmental Area (VTA) is a midbrain region implicated in a variety of motivated behaviors. However, the function of VTA GABAergic (Vgat+) neurons remains poorly understood. Here, using three-dimensional motion capture, *in vivo* electrophysiology, calcium imaging, and optogenetics, we demonstrate a novel function of VTA$^{\mathrm{Vgat+}}$ neurons. We found three distinct populations of neurons, each representing head angle about a principal axis of rotation: yaw, roll, and pitch. For each axis, opponent cell groups were found that increase firing when the head moves in one direction, and decrease firing in the opposite direction. Selective excitation and inhibition of VTA$^{\mathrm{Vgat+}}$ neurons generate opposite rotational movements. Thus, VTA$^{\mathrm{Vgat+}}$ neurons serve a critical role in the control of rotational kinematics while pursuing a moving target. This general-purpose steering function can guide animals toward desired spatial targets in any motivated behavior.

eTOC blurb

Hughes *et al*. demonstrate that VTA GABAergic projection neurons send reference commands for head angles. They describe neurons representing head angles for each of the three principal axes of rotation: yaw, roll and pitch. These results reveal a general mechanism for spatially precise steering that can be used in any motivated behavior.

Graphical Abstract

Lead contact: Henry H. Yin, hy43@duke.edu.

Author contributions: R.N.H. and H.H.Y. conceptualized and designed studies. R.N.H performed surgeries, behavioral experiments, electrophysiological recordings and calcium imaging. G.D.R.W. performed immunohistochemistry, confocal imaging, and helped design figures. N.K developed the tracking task. N.K, K.I.B., E.A.P., and R.N.H. wrote data collection and analysis code. K.I.B. captured and edited videos. R.N.H. and H.H.Y. drafted the manuscript. K.I.B., G.D.R.W., E.A.P., R.N.H. and H.H.Y edited and revised the manuscript. All authors have read and approved the manuscript.

Declaration of interests: The authors report no biomedical financial interests or potential conflict of interest

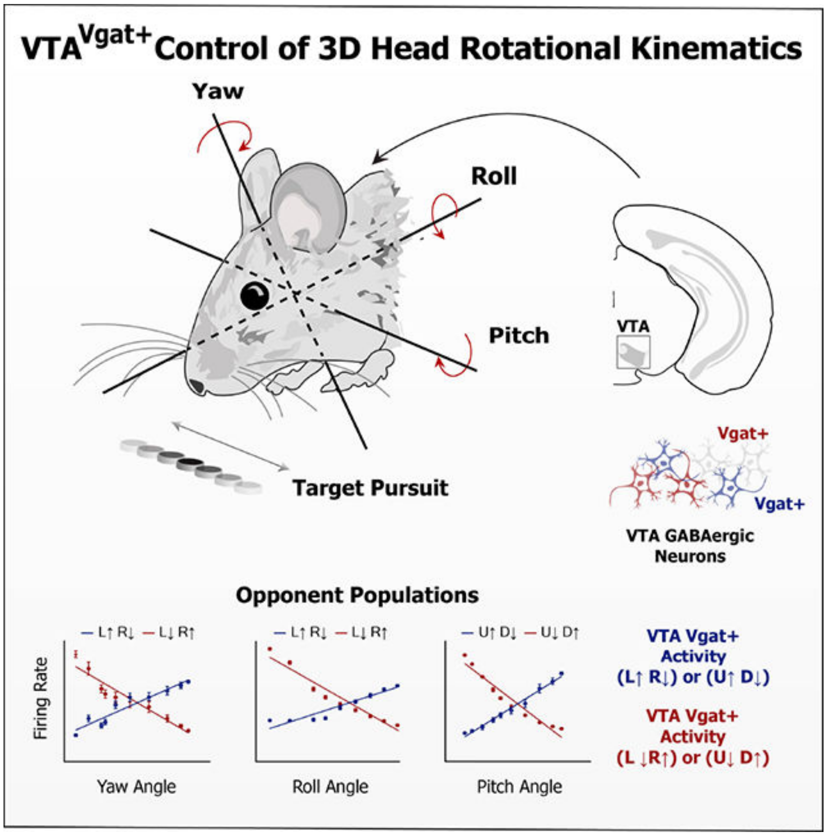

Introduction

The ventral tegmental area (VTA) has been implicated in motivated behaviors, addiction, and psychiatric disorders. Yet despite decades of research, the functional significance of the VTA is still poorly understood. Much research has focused on investigating the function of VTA dopamine neurons [1, 2]. By comparison, fewer studies have investigated VTA gamma-aminobutyric acid (GABA) neurons, the other main cell type in the VTA [3–6]. Importantly, the GABAergic population contains many projection neurons, which can inhibit their numerous downstream targets [7–9]. These projection neurons represent a major output of the limbic basal ganglia circuits.

VTA GABA neurons are thought to serve a role in aversive or defensive behaviors[5, 10], or to be involved in computing reward prediction errors [1]. Optogenetic activation of VTA GABA neurons disrupts reward-consumption [6]. In addition, putative VTA GABA neurons have also been found to correlate with locomotion[11, 12]. Clearly, VTA GABA neurons contribute to diverse behaviors, reflecting the heterogeneity of their anatomical connectivity. In this study, we used a novel continuous reward pursuit task to study the contribution of VTA GABA neurons to behavior, combining three-dimensional motion capture, electrophysiology, calcium imaging, and optogenetics.

Results

We wirelessly recorded single-unit activity in the VTA ($n = 479$ neurons, $n = 20$ mice) while mice performed a reward-tracking task during three-dimensional motion capture [13–16]. Because neurons in the VTA are difficult to classify based solely on spike waveform width and firing rate [17, 18], we confirmed our classification using optotagging in 6 mice, combining optogenetic activation and simultaneous electrophysiological recording. To selectively target inhibitory GABAergic neurons, we used the vesicular GABA transporter transgenic mice with Cre recombinase expression (*Vgat-ires-Cre)*. We stimulated channelrhodopsin (ChR2) infected VTA$^{\mathrm{Vgat+}}$ neurons in *Vgat-ires-Cre* mice while recording their single-unit activity ($n = 18$ neurons, Figure 1). Results from our opto-tagging experiments revealed distinct waveforms compared to the remaining population. Using an unsupervised clustering algorithm based on the first 10 principal components of the average waveforms, we identified two separate clusters. One of these clusters contained all of the optically identified GABAergic neurons, and was subsequently used to identify the remaining GABAergic population (Figures 1F–H).

During the reward-tracking task (Figures 2A and S1A), water-deprived mice were trained to continuously track a moving spout to receive a reward (12 μl of 10 % condensed milk, variable velocity at 5–50 mm/s). The spout moved continuously along either the horizontal (left and right) or vertical (up and down) axis during each session (Figures 2A and S2B). Rewards were continuously delivered every 500 ms if the mouse's head was sufficiently close to the moving spout, defined by the following distances: X axis: 30 mm, Y axis: 20 mm, and Z axis: 30 mm from the reward spout. There were no discrete trials or cues that predicted rewards. When the mice stopped tracking, the spout continued to move but no rewards were delivered. Kinematic data was extracted from markers placed on the head by infrared cameras, allowing quantification of behavioral variables such as position, velocity, acceleration, and head angle changes during behavior.

During reward tracking, mice showed a characteristic head rotation about three principal axes: yaw, roll, and pitch (Figure 2B, Videos S1, S2, and S3). During horizontal spout movement, mice significantly altered the roll and yaw angle of their head in a rhythmic fashion depending on the location of the spout (Videos S1 and S2), while the pitch angle largely stayed the same. On the other hand, during vertical spout movement, the pitch angle would fluctuate significantly, but the roll and yaw angles remained relatively constant (Video S3).

To understand the relationship between VTA GABA activity and continuous behavior, we compared single unit activity with a number of recorded behavioral variables including the pitch, yaw, and roll angles (Figures S1C–E). We discovered that the firing rates of many recorded neurons exhibited extremely high correlations with instantaneous head angles (Figures 2C–H and S2). Strikingly, we were able to identify three distinct classes of VTA GABA neurons corresponding to the yaw, roll, and pitch axes of rotation (Figure 2).

For each class of neurons, the firing rate varied monotonically with the head angle, and was selective for a single axis of rotation (Figures 2C–H). For example, a given neuron would increase its firing rate when the head was tilting to the left, and decrease firing when tilting to the right (Figure 2E). For each axis of rotation, we found two opponent populations based on the direction of rotation (Figure 3; Figure S3). There are thus six distinct populations of VTA GABA neurons related to instantaneous head angle. These correlations were extremely robust, and the linear relationship between firing rate and head angle was apparent even without averaging (Figure S2). A neuron that represents one axis of rotation would show weaker correlation with the other axes (Figures 4A–C). For both roll and yaw angle neurons, we found more neurons whose firing rates increased in the ipsiversive direction relative to the recording hemisphere (Figures 4I–J). Because the yaw and roll rotations co-varied when the animals were following a horizontally moving target, we compared their correlations with neural activity directly. For roll neurons, the average correlation with roll angle was significantly stronger than correlation with yaw angle (Figure 4B). This difference was also found for neurons classified as yaw neurons when compared to roll angle (Figure 4C). In order to examine whether we could predict head angle from all GABAergic neurons and not just those classified as head angle neurons, we used a machine learning algorithm (Support Vector Regression, SVR). With the SVR, we were able to decode actual head angle from all simultaneously recorded VTA neurons (Figure S4).

Next, we examined the activity of these head angle neurons at the time of reward delivery. Interestingly, the correlation between neural activity and head angle is degraded at the time of reward. Independently of their angle representation or direction preference, the neurons often show a very transient increase at the time of reward delivery (Figures 3D–F; Figures S3G–L). The response at reward delivery is similar to what was previously reported [17].

To further confirm that recorded neurons are GABAergic, we injected the fluorescent calcium indicator GCaMP7f into the VTA of *Vgat-ires-Cre* mice and used a miniature 1-photon microscope for chronic *in vivo* imaging (Figure 5A)[19–21]. This allowed us to simultaneously record calcium fluctuations ($n = 158$) and behavior. Consistent with our electrophysiological data, we found GABAergic neurons that were correlated with yaw, roll, and pitch (Figure 5; Figure S5). In addition, we found more yaw and roll neurons that increased their firing rates in the ipsiversive direction relative to the hemisphere being imaged (Figure S5I).

VTA GABA activity usually preceded head angle change (Figures 4D–G, Yaw: 117 ± 54 ms; Roll: 55 ± 23 ms; Pitch: 76 ± 29 ms). This suggests that these neurons send top down commands to generate movements with the specified rotational kinematics. To test this hypothesis, we used optogenetics to manipulate $\text{VTA}^{\text{Vgat+}}$ neurons, using ChR2 for excitation or soma-targeted *Guillardia theta* anion-conducting ChR2 (stGtACR2) for inhibition (Figure 6A; $\text{Vgat::ChR2}^{\text{VTA}}$, $n = 6$; $\text{Vgat::stGtACR2}^{\text{VTA}}$, $n = 6$; control, $\text{Vgat::eYFP}^{\text{VTA}}$, $n = 7$). We found that both optogenetic excitation and inhibition of $\text{VTA}^{\text{Vgat+}}$ neurons produce opposite head rotations in all three axes (Figures 6C–D, Figures S6 and S7). During excitation, the head is lowered (pitch angle decreased relative to the longitudinal axis of the body), and the roll and yaw angles deviate towards the stimulated hemisphere (Figures 6C–D; Video S4). There is therefore a predominantly ipsiversive effect on head angle. During inhibition, the head is raised (increased pitch angle), and the roll and yaw angles deviated away from the stimulation hemisphere, showing a contraversive effect

(Figures 6C–D, Video S5). These results agree with our electrophysiology and imaging results. Strikingly, parametric manipulations of pulse width quantitatively determined head angle (Figure 6C). The latency between stimulation and behavioral changes was approximately the same for each axis of rotation (Figures S6G–I, Yaw: 37 ± 5 ms; Roll: 37 ± 4 ms; Pitch: 39 ms ± 6 ms). In addition, pulse frequency manipulations with ChR2 showed a linear relationship between frequency and head angle (Figures S6D–F).

Furthermore, selective optogenetic excitation of $\text{VTA}^{\text{Vgat+}}$ neurons reduced reward consumption, as previously reported [6]. This appeared to be caused by an increase in the distance between their head and the spout during stimulation (Figure 7K). Using our stimulation parameters, there did not appear to be significant aversion induced by photo-stimulation. We confirmed this in a real-time place preference assay, in which entering one side of the arena results in sustained optogenetic stimulation of the $\text{VTA}^{\text{Vgat+}}$ neurons (Figure 7).

Discussion

Collectively, our results show for the first time that VTA GABA neurons represent rotational kinematics of the head, and shed light on the computational role of these neurons. The major advantage of our approach is the lack of head restraint, so that the relationship between neural activity and free behavior is revealed for the first time. We found three distinct classes: the instantaneous firing rate of each preferentially represents a separate angle (yaw, roll, and pitch). Furthermore, each class can be further divided into populations that increase firing in a given head tilt direction. It appears that each population is primarily responsible for tilt in a single direction. In order to achieve bi-directional control within the system, opponent populations are needed to increase or decrease head angle about a particular axis of rotation. Moreover, our findings show that VTA GABA neurons not only represent head angles, but also generate desired angles during continuous behavior. This is possible if their output, acting as reference signals, quantitatively dictate the sensory states to be reached by lower level control systems [22, 23].

While our results demonstrate the role of VTA GABA neurons in control of head orientation, it does not follow that this is their sole function. Much like their neighboring dopamine neurons, GABA neurons receive a diverse set of inputs and have wide-ranging connections to many different brain regions, suggesting that they could be functionally heterogeneous [7, 24].

Given the popular view that the VTA is crucial for motivated behaviors, one obvious question is how the present findings could be related to the previous literature. A few studies have examined the role of the VTA GABA neurons in behavior using cell-type specific manipulations. However, because they either relied on head-fixed preparations, or used behavioral measures such as place preference, average speed, or distance traveled, they were not able to show the coordination of head rotation kinematics we demonstrate here [5, 6].

Previous studies found that stimulation of VTA GABA neurons interrupted reward consumption. This is not surprising given our finding that optogenetic manipulation of these neurons predictably resulted in head deviation. Even in head-fixed mice, it is possible that such deviations are sufficient to interrupt reward consumption. We also found that consumption was reduced during optogenetic stimulation, primarily due to stimulation-induced head rotation, which increases distance from the reward spout (Figure 7K).

A popular hypothesis used to explain the role of VTA dopamine neurons is the reward prediction error hypothesis based on the reinforcement learning paradigm [25]. According to this hypothesis, phasic dopamine activity reflects the difference between actual and predicted rewards. Previous work also suggests that, by inhibiting DA neurons, VTA GABA neurons could perform a subtraction needed for calculation of prediction errors [1]. While our results do not rule out this role, they show for the first time that these neurons directly command the actual behavior in a spatially precise manner (Figure 6). Our task design allowed us to disassociate reward prediction error from head rotation. There is no conditioned stimulus that predicted reward delivery; rather the mice received rewards continuously as long as they were pursuing the target. Their expectation of reward was thus identical regardless of the direction of pursuit.

In addition, several features of our results are incompatible with the reward prediction error hypothesis. First, the three principal axes of rotation are independent of reward prediction. Second, for each axis of rotation, VTA GABA neurons displayed clear direction selectivity, and opponent signaling: for example, we found two opponent populations of yaw neurons, one increasing firing with leftward tilt and the other increasing firing with rightward tilt (Figure 3C). This is consistent with what has previously been found in the substantia nigra [26–28]. Finally, we found that the effective zero (no rotation or neutral position) for the rotation-related neurons is found close to the middle of the range of firing rates (Figure 3C), which explains the tonic firing rate of VTA GABA neurons. Increases and decreases from this zero value represent the signals related to rotation about a particular axis[15, 28]. No version of the reward prediction error hypothesis predicts these features. Reinforcement learning in general does not attempt to address how behavior is actually generated. The behavioral policies in such models are all-ornone (action or no action), rather than continuous (degree of tilt in a given direction along a given axis) and spatially defined. It should also be noted that, given the strong connections between GABAergic and dopaminergic neurons in the VTA, it is possible that the dopaminergic neurons would also play a role in controlling head orientation. Previous work demonstrated that dopaminergic neurons in the neighboring substantia nigra pars compacta can signal movement velocity in a direction-specific manner [29], but the role of VTA dopaminergic neurons in movement remains poorly defined. Future studies will be needed to understand the interaction between different cell types in the VTA and their coordinated contributions to behavior.

Our results also suggest that a separate process related to the consummatory phase of behavior may take over and command VTA neurons at the time of reward. This may explain why activity at the time of reward delivery is often seen in these neurons, and why the correlations with head angle seem to be degraded at the time of reward receipt (Figures 3D–F and S3G–L). The mechanisms underlying the appetitive and consummatory phases of motivated behaviors must be precisely coordinated and overlap in time to achieve smooth control.

While head rotation control is essential for most motivated behaviors, it has largely been neglected in previous studies. Brain systems for precise orienting and steering are necessary for nearly all aversive and appetitive behaviors, whether seeking reward or avoiding harm. For example, in consummatory behavior such as eating, the mouse must make continuous and subtle adjustments of the head. Furthermore, all escape behaviors require rapid orienting movements in order to successfully evade threatening stimuli. Thus, conflicting previous findings on the contribution of the VTA to appetitive and aversive processes are consistent with a more general role in orientation and steering, as suggested by our findings. Our results could also explain why others have found that optogenetic excitation of VTA GABA neurons is aversive[5]. Excessive vestibular disturbance, for example, can be highly aversive and can result in disorientation and nausea. Indeed, during our optogenetic experiments, the mice sometimes showed urination and defecation in addition to the head angle changes. However, it is unclear that activation of VTA GABA neurons within their physiological firing rates produces aversion. Neurons that we classified as GABAergic had an average firing rate of 20.3 ± 1.04 Hz, consistent with what has previously been reported[17]. Our stimulation parameters therefore were more physiological (10–40 Hz) than those used in previous work (constant stimulation), which could also explain the lack of a clear aversive effect here [5]. Furthermore, it has also recently been discovered that constant light stimulation over several seconds can produce inhibition in neurons without opsins due to excessive heat[30]. As a result, constant stimulation used in previous work could introduce a significant confound of other VTA neuronal populations being inhibited.

Implementing fine control of the head, given the multiple degrees of freedom involved, presents a significant computational challenge. Our results suggest that the brain solves this control problem using a similar strategy found in airplanes or ships, using independent control of three orthogonal axes of rotation. Distinct neuronal populations in the VTA are responsible for independent control of rotation along pitch, yaw, and roll. The observation that activity in these cells generally leads the kinematic variable suggests that VTA neurons do not simply provide perceptual representations of head angle. The signals are not predictions of future perceptual signals, but commands that dictate the perceptions to be reached, as demonstrated by our optogenetic stimulation results[23]. The amount of stimulation quantitatively determines the head angle achieved (Figures 6 and S6). In normal movements, presumably all the populations are engaged, though to different extents depending on the degree of rotation along each axis.

Interestingly, the VTA is directly connected to key nuclei in the head direction circuit[31, 32]. Angular head velocity cells have been reported in the dorsal tegmental nucleus, superior colliculus, and the lateral habenula, which are all connected to the VTA[9, 32–34]. Thus, VTA neurons are in a position to integrate signals representing angular head velocity and generate head angle representations. The interactions between the VTA and the other components of the head steering circuit remain to be investigated.

While our results shed light on the computational role of VTA GABAergic neurons, it is important to note that there are important methodological limitations in our task design. For example, the animal’s head movements were restricted to a relatively small degree of head rotation relative to their natural capabilities. In addition, many behavioral variables, such as whisker deflection or visual input, could potentially introduce confounds, and thus need to be further investigated in future work.

STAR Methods

Lead Contact and Materials Availability

Further information and requests for resources should be directed to the Lead Contact, Dr. Henry Yin (hy43@duke.edu). This study did not generate new unique reagents.

Experimental Model and Subject Details

All experimental procedures were approved by the Animal Care and Use Committee at Duke University. Both male and female C57BL/6J and *Vgat-ires-Cre* mice (3–8 months) acquired from Jackson Laboratory were used. Mice were maintained on a 12:12 light cycle and tested during the light phase. Mice used for *in vivo* electrophysiology and calcium imaging experiments were singly housed. All other mice were group housed. During behavioral experiments, mice were placed on water restriction. After training sessions, mice had free access to water for approximately 2 hours and were maintained at approximately 85–90% of their initial weights.

Method Details

Viral Constructs—rAAV5.EF1α.DIO.hChR2(H134R).eYFP and rAAV5.EF1α.DIO.eYFP were obtained from the Duke University Vector Core. pAAV-hSyn1-SIO-stGtACR2-FusionRed (Mahn et al., 2018) and pGP-AAV-syn-jGCaMP7f-WPRE (Dana et al., 2018) were obtained from Addgene. pGP-AAV-syn-jGCaMP7f-WPRE was from Douglas Kim (Addgene viral prep # 104488-AAV1; http://n2t.net/addgene:104488; RRID:Addgene_104488). pAAV_hSyn1-SIO-stGtACR2-FusionRed was from Ofer Yizhar (Addgene viral prep # 105677-AAV1; http://n2t.net/addgene:105677; RRID:Addgene_105677).

Surgery—Mice were anesthetized with 2.0 to 3.0% isoflurane mixed with 0.60 L/min of oxygen for surgical procedures and placed into a stereotactic frame (David Kopf Instruments, Tujunga, CA). Meloxicam (2 mg/kg) and topical bupivacaine (0.20 mL) were administered prior to incision. C57BL/6J mice ($n = 26$; 14 males, 12 females) were used for electrophysiology experiments. 16 channel electrode arrays (4×4 fixed or drivable) were lowered into the VTA (AP: 3.2 – 3.4 relative to bregma, ML: 0.4 – 0.6 relative to bregma, DV: 4.0 – 4.4 relative to brain surface) at a rate of 300 μm/min and grounded to a cranial crew. For optrode experiments, 200 nL of DIO-ChR2 was unilaterally injected into the VTA (AP: 3.2 – 3.4 relative to bregma, ML: 0.4 – 0.6 relative to bregma, DV: 4.0 – 4.4 relative to brain surface) of *Vgat-ires-Cre* mice using a microinjector (Nanoject 3000, Drummond Scientific) at a rate of 1 nL/s. The pipette was left to sit for 10 minutes at the injection site to allow absorption of the virus and prevent leakage. Optrodes were 4×4 microwire arrays (Neurophysiology Instruments) with a custom-made optic fiber positioned at an angle on the long side of the connector to maximize the number of neurons stimulated under the electrode array (Sparta et al., 2012). For optogenetic stimulation experiments, 200–300 nL of either AAV-DIO-ChR2 for excitation or AAV-SIO-stGtACR2 for inhibition was bilaterally injected into the VTA of *Vgat-ires-Cre* mice (*n* = 23; 11 males, 12 females) using the coordinates previously described. Custom-made optic fibers (5 – 6 mm length below ferrule, >80% transmittance, 105 μm core diameter) were then implanted directly above the VTA at an angle (AP: 3.2 – 3.4 with respect to bregma, ML: 1.6 with respect to bregma, DV: 3.8 from the brain surface; 15°). Fibers and electrodes were secured in place with dental acrylic adhered to skull screws. For calcium imaging experiments, *Vgat-ires-Cre* mice (*n* = 7; 3 males, 4 females) were unilaterally injected with 400 nL of AAV1-syn-jGCaMP7f-WPRE into the VTA at the coordinates and injection parameters previously described. A gradient-index (GRIN) lens (Inscopix, 0.6mm × 7.1mm) was then slowly implanted above the VTA (AP: −3.2 – 3.5 with respect to bregma, ML: 0.4 – 0.8 with respect to bregma, DV: 4.0 from the brain surface) over the course of an hour. The lens was secured to implanted cranial screws with dental cement and covered with Kwik-Sil silicone elastomer (World Precision Instruments) to protect the surface of the lens. All mice were fitted with a headbar that holds infrared markers for motion capture. Both heterozygous and homozygous *Vgat-ires-Cre* mice were used. Mice were allowed to recover for two weeks after surgery before experimentation.

Behavioral Tasks and Analysis

Reward Tracking Task: Mice were placed on a custom-built platform (40 cm tall) and the platform was placed several cm away from a spout that was controlled by a stepper motor (Bipolar, 56.3 × 56.3 mm, DC 1.4A, 2.9Ω, 1.8 degree / step, Oriental motor, USA). To track movement, two infrared reflective markers (B & L Engineering) were attached to each side of a custom-made head bar attached to the dental cement skullcap of mice. A third marker was attached to either the top of the wireless electrode head stage, the top of the miniscope, or on a third bar attached to the skullcap. The reward position was tracked by placing a reflective marker approximately 20 mm away from the reward spout. Eight Raptor-H Digital infrared cameras were used to capture the movement of reflective markers during tracking. The data was then processed in Cortex (Motion Analysis, CA) and converted into Cartesian coordinates. Both reward delivery and the movement of the reward spout were controlled using custom MATLAB scripts. The program would deliver a 10% solution of condensed milk (12 μl every 500 ms) if mice tracked the moving spout (5–50 mm/sec) within a narrow window of Cartesian coordinates (X axis: 30 mm, Y axis: 20 mm, Z axis: 30 mm from the reward spout marker. During three-dimensional motion capture, the reflective markers on the head were used to compute angle changes. When the angles are zero, the animal’s head is flat and in a ‘neutral’ position. To calculate the changes in roll and yaw angles, the position coordinates for a single axis were obtained from the three-dimensional motion tracking software. The absolute distance between the markers (one on each side of the head) allowed calculation of the adjacent length of a triangle. Once all vector coordinates were obtained for one axis (e.g. x-axis), the change in marker position was computed for each time step, providing the opposite length of the triangle. As the distance between markers is the adjacent length, the arc tangent was then computed and converted into degrees for instantaneous angle changes using a custom MATLAB script. For pitch angle, the two side head bar markers and the third top marker created a triangle in three-dimensional Cartesian space. Given the midpoint between two side markers, the MATLAB function that converts

Cartesian coordinates to spherical coordinates (car2sph) was used to compute the instantaneous pitch angle.

Real Time Conditioned Place Preference: Mice were placed on one side of a rectangular open field arena (45 cm L, 25 cm W, 35 cm H) that was partitioned in the middle by two 8 cm wide walls with a 9 cm opening. Videos were recorded with a camera that was placed 0.7 meters above the chamber and connected to a computer. Two-dimensional coordinates based on the center of mass of each mouse were collected at 50 f/s. An open source software program (Bonsai) using a custom script tracked movements for 30 minutes[35]. A session consisted of 3 separate, 10 min epochs: a pre-stimulation epoch with no stimulation, a stimulation epoch where unilateral stimulation occurred only if the mice were on one half of the arena, and a post-stimulation epoch of no stimulation. Stimulation was produced using a laser attached to two Arduinos: one received commands from the computer, and the other controlled the frequency output of the laser using TTL pulses. Data were analyzed using a custom Matlab script.

Wireless in Vivo Electrophysiology—For electrophysiological recordings, either 4×4 16-channel fixed electrode ($n = 23$) or drivable 16-channel arrays ($n = 3$) (Innovative Neurophysiology, Inc.) were used. Driveable electrodes were moved 50–100 μm each session. If neurons in the same channel displayed a significantly similar waveform and ISI distribution after electrodes movement, they were excluded from analysis. Fixed arrays were constructed of tungsten wires (35 μm diameter, 150 μm spacing, 5–6 mm length). Drivable electrodes were single-drive movable micro-bundles (1 × 16) with 23 μm diameter electrodes driven through a guide cannula. VTA neural recordings were performed as previously described. Briefly, a miniaturized wireless head stage (Triangle Biosystems) or a tethered headstage interfaced with a Cerebrus data acquisition system (Blackrock Microsystems) was used to record activity during freely moving behavior. Electrophysiology Data were filtered with both analog and digital bandpass filters (analog highpass 1st order Butterworth filter at 0.3 Hz, analog lowpass 3rdorder Butterworth filter at 7.5 kHz, digital highpass 4th order Butterworth filter at 250 Hz). Filtered data was then sorted using Offline Sorter (Plexon) and analyzed Neuroexplorer (Nexus). To qualify as single unit activity, the signal must have had a 3:1 signal-to-noise ratio, a refractory period of at least 800 μs and consistent waveforms throughout the session.

Optogenetic Stimulation and three-dimensional Motion Tracking—*Vgat-ires-cre* mice were used for optogenetic stimulation experiments. Unilateral stimulation data were taken from the same bilaterally implanted animal on separate experimental days. The output from the optic fiber tip was measured (PM120VA, ThorLabs) before each experimental session to obtain a power between 8–12 mW (i.e. ~10 mW power delivered to the stimulation site with a transmittance of ~85%). A MATLAB program interfaced to a National Instruments DAQ triggered square pulse (5 ms – 500 ms). Head movements were captured at 100 Hz in a Cartesian plane with eight Raptor-H digital infrared cameras (Motion Analysis, CA). To calculate the deviation of the head angle for pitch, roll, and yaw due to optogenetic stimulation, we first recorded the head angle during the 100 ms window prior to stimulation, and then compared it to the asymptotic level of head angle 100 ms after stimulation, or 200 ms after the end of the stimulation. For latency between stimulation and head angle changes, a 500 ms baseline was used for comparison.

In Vivo Calcium Imaging—Approximately 3 weeks after viral injection, fluorescence was checked using a custom modified UCLA miniscope designed to hold a relay lens (1.8× 4.3 mm, Edmund Optics)[19]. A baseplate was then fixed over the implanted GRIN lens using dental cement. During behavioral testing, one reflective marker was adhered to top of the miniscope, and two were adhered to the side of the head bar to obtain pitch, roll and yaw angles. For calcium imaging analysis, all videos were preprocessed using Mosaic (Inscopix) for motion correction and spatial binning, and then subsequently analyzed using a custom MATLAB Script. Data were then processed using a constrained non-negative matrix factorization (CNMF analysis) for denoising, deconvolving and demixing the data [36]. This method subtracts out background fluorescence, and accurately localizes and segregates neuronal activity (CNMF Parameters: data was captured and analyzed at 30 frames per second; minimum PNR ratio was 10% below maximum for each animal, with an average of 8; minimum correlational value was 10% below maximum for each animal, with an average of 0.85. The gSiz ranged from 10–20, with the gSig range of 3 to 10). Neuroexplorer was then used to analyze calcium activity and behavioral variables.

Histology—To confirm viral expression and optic fiber and electrode placement, mice were transcardially perfused with 0.1M phosphate buffered saline (PBS) followed by 4% paraformaldehyde (PFA). To aid placement, heads were stored in 4% PFA with 30% sucrose for 72 hrs. Brains were then post-fixed for 24 hours in 30% sucrose prior to cryostat sectioning (Leica CM1850) at 60 μm coronally. Fiber, electrodes, and lens implantation sites were verified after sections were processed for the presence of cytochrome oxidase to visualize cytoarchitecture by rinsing in 0.1M PB before incubating in a diaminobenzidine, cytochrome C, and sucrose solution for ~2 hours at room temperature. Mounted cytochrome oxidase sections were then dehydrated in 200 proof ethanol, defatted in xylene, and coverslipped with cytoseal. To confirm eYFP and FusionRed coexpression in VTA *Vgat+* cells, as well as labeling in the vicinity of dopaminergic cells of *Vgat-ires-Cre* transgenic mice, select sections were rinsed in 0.1M PBS for 20 min before being placed in a PBS-based blocking solution containing 5% goat serum and 0.25% Triton X-100 at room temperature for 1 hr. Sections were then incubated with a primary antibody (polyclonal rabbit anti-Vgat, 1:200 dilution, ThermoFisher, catalog no. PA5–27569; polyclonal rabbit anti-Dopamine transporter, 1:200 dilution, abcam, catalog no. 18441; polyclonal rabbit anti-Tyrosine hydroxylase, 1:200 dilution, Millipore, catalog no. AB152) in blocking solution overnight at 4 °C. Sections were then rinsed in PBS for 20 min before being placed in a secondary antibody used to visualize *Vgat, DAT,* or *TH* neurons in the VTA (goat anti-rabbit Alexa Fluor 594, 1:1000 dilution, abcam, catalog no. ab150080; goat anti-rabbit Alexa Fluor 488, 1:1000 dilution, abcam, catalog no. ab150077) for 1 hr at room temperature. Sections for fluorescent microscopy were mounted and immediately coverslipped with Fluoromount G with DAPI medium (Electron Microscopy Sciences; catalog no. 17984–24). Brightfield images for placement verification were acquired and stitched using an Axio Imager.M1 upright microscope (Zeiss) and fluorescent images were acquired and stitched using a Z10 inverted microscope (Zeiss) (Figure S8).

GABAergic Neuron Classification—We used a Gaussian mixture model (GMM; Python sklearn package) to perform unsupervised clustering of neurons for classification without explicitly selecting a threshold, thus reducing bias. To perform this analysis, the mean waveforms were first normalized and fit with a principal component analysis. The top 10 components, which explained over 95% of the variance, were clustered using a GMM. Classifications were then used to analyze putative GABAergic neurons that were not optically tagged.

Support Vector Regression Decoder—Roll and yaw angle were decoded from the same horizontal tracking sessions, whereas pitch was decoded from a vertical tracking task. All of the data was binned into 50 ms intervals, and fit using support vector regression. As the number of neurons and the size of the training data can affect decoding performance, we limited our analysis to sessions where we had at least 6 classified GABAergic neurons, and at least 3.5 minutes of training data. For each of these sessions the model was trained on the first 60% of the data, and performance was evaluated on a contiguous set of held-out data (15%). Prior to fitting the model, the neural data was z-scored, and the head-angles were zero-centered. Using these methods, we were able to achieve good decoding performance, considering our relatively short sessions, and limited number of neurons [37].

Quantification and Statistical Analyses

All statistical analyses were performed in MATLAB and GraphPad Prism. A power analysis was not conducted to determine sample size *a priori.*

Correlation Analyses for Peri-event raster plots—Data were aligned either towards the spout moving in the rightward or downward direction, and were binned in 50 ms windows and Gaussian smoothed with a filter width of 5 bins, within a total window of 5 s in Neuroexplorer using a peri-event raster. Output data were then sorted according to the minimum and maximum head angles and the corresponding neural activity and collapsed into 10 data points each. These data were then exported into GraphPad Prism, where a correlation analysis was performed. For population analyses, neural data and behavioral variables binned at 50 ms were normalized using a Z-score analysis performed using a custom MATLAB script. The normalized data from each animal were then averaged together, where a population average was obtained for both the behavioral variables and the neural data. For correlation analysis with calcium imaging data, the analysis was identical to the one described above, but data were binned at 100 ms and Gaussian smoothed with a filter width of 10 bins. To classify neurons as pitch, roll, or yaw, the highest correlational value between neural data and the relevant behavioral variable was chosen.

Correlation Analyses Across Entire Behavioral Session—For each animal, neural data and continuously monitored yaw, roll, or pitch behavioral variables for the entire recording session were constructed using 10 ms time bins in NeuroExplorer and exported to MATLAB. Behavioral variables and neural activity were sorted according to magnitude (40 bins), and a Pearson Correlation between them was performed. For selected neurons, neural activity and behavioral variable information were filtered to exclude data when the animal was not tracking the reward spout. For shuffled data, we took behavioral variables and corresponding neural activity in 10 ms bins and used the Matlab function randperm to shuffle the data before analyzing the correlation between neural activity and behavior.

Cross-Correlation Analyses—For each animal, neural data and continuously monitored roll, yaw, or pitch behavioral variables for the entire recording session were extracted as described above. Using the behavioral variables and identified yaw, roll and pitch neurons from the correlation analyses, a custom MATLAB script was then utilized to perform cross-correlation analyses between the continuously monitored behavioral variables and neural activity. Cross-correlations were performed using MATLAB's *xcorr* function, using the behavioral variable as the reference time-series, and the neural data as the shifted time series. Latencies were determined by finding the lag to the maximum value of the cross-correlation for positively correlated neurons and the lag to the minimum value for anti-correlated neurons. Cross-correlations were Z-score normalized and averaged together across data sets from all animals to obtain population data.

Data and Code Availability

Raw data from the current study were not deposited into a public repository due to the large size of the data sets, but are available from the corresponding author upon request.

Supplementary Material

Refer to Web version on PubMed Central for supplementary material.

Acknowledgments

We would like to thank Dr. Fengxia Allen, Dr. Guozhong Yu, Dr. Joseph Barter, Dr. Jinyong Zhang, Lee Christensen, and Murray Wickwire for their technical assistance. We would like to thank Dr. Joseph Barter for helpful comments and discussions. We also thank Dr. Nicole Calakos and Dr. Brandon Turner for providing the gCaMP7f virus. This work was supported by NIH grants DA040701, NS094754 and MH112883 to HHY.

References

1. Eshel N, Bukwich M, Rao V, Hemmelder V, Tian J, and Uchida N (2015). Arithmetic and local circuitry underlying dopamine prediction errors. Nature 525, 243–246. [PubMed: 26322583]
2. Lammel S, Lim BK, and Malenka RC (2014). Reward and aversion in a heterogeneous midbrain dopamine system. Neuropharmacology 76 Pt B, 351–359. [PubMed: 23578393]
3. Fields HL, Hjelmstad GO, Margolis EB, and Nicola SM (2007). Ventral tegmental area neurons in learned appetitive behavior and positive reinforcement. Annual review of neuroscience 30, 289–316.
4. Nair-Roberts RG, Chatelain-Badie SD, Benson E, White-Cooper H, Bolam JP, and Ungless MA (2008). Stereological estimates of dopaminergic, GABAergic and glutamatergic neurons in the ventral tegmental area, substantia nigra and retrorubral field in the rat. Neuroscience 152, 1024–1031. [PubMed: 18355970]
5. Tan KR, Yvon C, Turiault M, Mirzabekov JJ, Doehner J, Labouebe G, Deisseroth K, Tye KM, and Luscher C (2012). GABA neurons of the VTA drive conditioned place aversion. Neuron 73, 1173–1183. [PubMed: 22445344]
6. van Zessen R, Phillips JL, Budygin EA, and Stuber GD (2012). Activation of VTA GABA neurons disrupts reward consumption. Neuron 73, 1184–1194. [PubMed: 22445345]
7. Beier KT, Gao XJ, Xie S, DeLoach KE, Malenka RC, and Luo L (2019). Topological Organization of Ventral Tegmental Area Connectivity Revealed by ViralGenetic Dissection of Input-Output Relations. Cell reports 26, 159–167 e156. [PubMed: 30605672]

8. Morales M, and Margolis EB (2017). Ventral tegmental area: cellular heterogeneity, connectivity and behaviour. Nature reviews. Neuroscience 18, 73–85.

9. Taylor SR, Badurek S, Dileone RJ, Nashmi R, Minichiello L, and Picciotto MR (2014). GABAergic and glutamatergic efferents of the mouse ventral tegmental area. The Journal of comparative neurology 522, 3308–3334. [PubMed: 24715505]

10. Zhou Z, Liu X, Chen S, Zhang Z, Liu Y, Montardy Q, Tang Y, Wei P, Liu N, Li L, et al. (2019). A VTA GABAergic Neural Circuit Mediates Visually Evoked Innate Defensive Responses. Neuron.

11. Puryear CB, Kim MJ, and Mizumori SJ (2010). Conjunctive encoding of movement and reward by ventral tegmental area neurons in the freely navigating rodent. Behavioral neuroscience 124, 234. [PubMed: 20364883]

12. Wang DV, and Tsien JZ (2011). Conjunctive processing of locomotor signals by the ventral tegmental area neuronal population. PloS one 6, e16528. [PubMed: 21304590]

13. Fan D, Rich D, Holtzman T, Ruther P, Dalley JW, Lopez A, Rossi MA, Barter JW, Salas-Meza D, Herwik S, et al. (2011). A wireless multi-channel recording system for freely behaving mice and rats. PLoS One 6, e22033. [PubMed: 21765934]

14. Bartholomew RA, Li H, Gaidis EJ, Stackmann M, Shoemaker CT, Rossi MA, and Yin HH (2016). Striatonigral control of movement velocity in mice. The European journal of neuroscience 43, 1097–1110. [PubMed: 27091436]

15. Kim N, Li HE, Hughes RN, Watson GDR, Gallegos D, West AE, Kim IH, and Yin HH (2019). A striatal interneuron circuit for continuous target pursuit. Nature communications 10, 2715.

16. Rossi MA, Fan D, Barter JW, and Yin HH (2013). Bidirectional Modulation of Substantia Nigra Activity by Motivational State. PloS one 8, e71598. [PubMed: 23936522]

17. Cohen JY, Haesler S, Vong L, Lowell BB, and Uchida N (2012). Neuron-type-specific signals for reward and punishment in the ventral tegmental area. Nature 482, 85–88. [PubMed: 22258508]

18. Margolis EB, Lock H, Hjelmstad GO, and Fields HL (2006). The ventral tegmental area revisited: is there an electrophysiological marker for dopaminergic neurons? J Physiol 577, 907–924. [PubMed: 16959856]

19. Cai DJ, Aharoni D, Shuman T, Shobe J, Biane J, Song W, Wei B, Veshkini M, La-Vu M, Lou J, et al. (2016). A shared neural ensemble links distinct contextual memories encoded close in time. Nature 534, 115–118. [PubMed: 27251287]

20. Dana H, Sun Y, Mohar B, Hulse B, Hasseman JP, Tsegaye G, Tsang A, Wong A, Patel R, Macklin JJ, et al. (2018). High-performance GFP-based calcium indicators for imaging activity in neuronal populations and microcompartments. bioRxiv, 434589.

21. Flusberg BA, Nimmerjahn A, Cocker ED, Mukamel EA, Barretto RP, Ko TH, Burns LD, Jung JC, and Schnitzer MJ (2008). High-speed, miniaturized fluorescence microscopy in freely moving mice. Nature methods 5, 935–938. [PubMed: 18836457]

22. Yin HH (2017). The Basal Ganglia in Action. Neuroscientist 23.

23. Yin HH (2014). How basal ganglia outputs generate behavior. Advances in neuroscience 2014, 768313.

24. Yu X, Li W, Ma Y, Tossell K, Harris JJ, Harding EC, Ba W, Miracca G, Wang D, Li L, et al. (2019). GABA and glutamate neurons in the VTA regulate sleep and wakefulness. Nature neuroscience 22, 106–119. [PubMed: 30559475]

25. Schultz W (1998). Predictive reward signal of dopamine neurons. Journal of neurophysiology 80, 1–27. [PubMed: 9658025]

26. Fan D, Rossi MA, and Yin HH (2012). Mechanisms of action selection and timing in substantia nigra neurons. The Journal of neuroscience : the official journal of the Society for Neuroscience 32, 5534–5548.

27. Barter JW, Castro S, Sukharnikova T, Rossi MA, and Yin HH (2014). The role of the substantia nigra in posture control. European Journal of Neuroscience 39 *(9)*, 1465–1473. [PubMed: 24628921]

28. Barter JW, Li S, Sukharnikova T, Rossi MA, Bartholomew RA, and Yin HH (2015). Basal ganglia outputs map instantaneous position coordinates during behavior. Journal of Neuroscience 35, 2703–2716. [PubMed: 25673860]

29. Barter J, Li S, Lu D, Rossi M, Bartholomew R, Shoemaker CT, Salas-Meza D, Gaidis E, and Yin HH (2015). Beyond reward prediction errors: the role of dopamine in movement kinematics. Frontiers in Integrative Neuroscience 9, 39. [PubMed: 26074791]
30. Owen SF, Liu MH, and Kreitzer AC (2019). Thermal constraints on in vivo optogenetic manipulations. Nature neuroscience 22, 1061–1065. [PubMed: 31209378]
31. Angelaki DE, and Yakusheva TA (2009). How vestibular neurons solve the tilt/translation ambiguity. Comparison of brainstem, cerebellum, and thalamus. Annals of the New York Academy of Sciences 1164, 19–28. [PubMed: 19645876]
32. Taube JS (2007). The head direction signal: origins and sensory-motor integration. Annual review of neuroscience 30, 181–207.
33. Bassett JP, and Taube JS (2001). Neural correlates for angular head velocity in the rat dorsal tegmental nucleus. The Journal of neuroscience : the official journal of the Society for Neuroscience 21, 5740–5751. [PubMed: 11466446]
34. Faget L, Osakada F, Duan J, Ressler R, Johnson AB, Proudfoot JA, Yoo JH, Callaway EM, and Hnasko TS (2016). Afferent Inputs to Neurotransmitter-Defined Cell Types in the Ventral Tegmental Area. Cell reports 15, 2796–2808. [PubMed: 27292633]
35. Lopes G, Bonacchi N, Frazao J, Neto JP, Atallah BV, Soares S, Moreira L, Matias S, Itskov PM, Correia PA, et al. (2015). Bonsai: an event-based framework for processing and controlling data streams. Front Neuroinform 9, 7. [PubMed: 25904861]
36. Pnevmatikakis EA, Soudry D, Gao Y, Machado TA, Merel J, Pfau D, Reardon T, Mu Y, Lacefield C, Yang W, et al. (2016). Simultaneous Denoising, Deconvolution, and Demixing of Calcium Imaging Data. Neuron 89, 285–299. [PubMed: 26774160]
37. Glaser JI, Chowdhury RH, Perich MG, Miller LE, and Kording KP (2017). Machine learning for neural decoding. arXiv preprint arXiv:1708.00909.

Highlight

3 classes of VTA GABA neurons represent pitch, yaw, and roll head angles

Two opponent neuronal populations for each axis of rotation based on direction

Optogenetic excitation and inhibition produce opposite rotational movements.

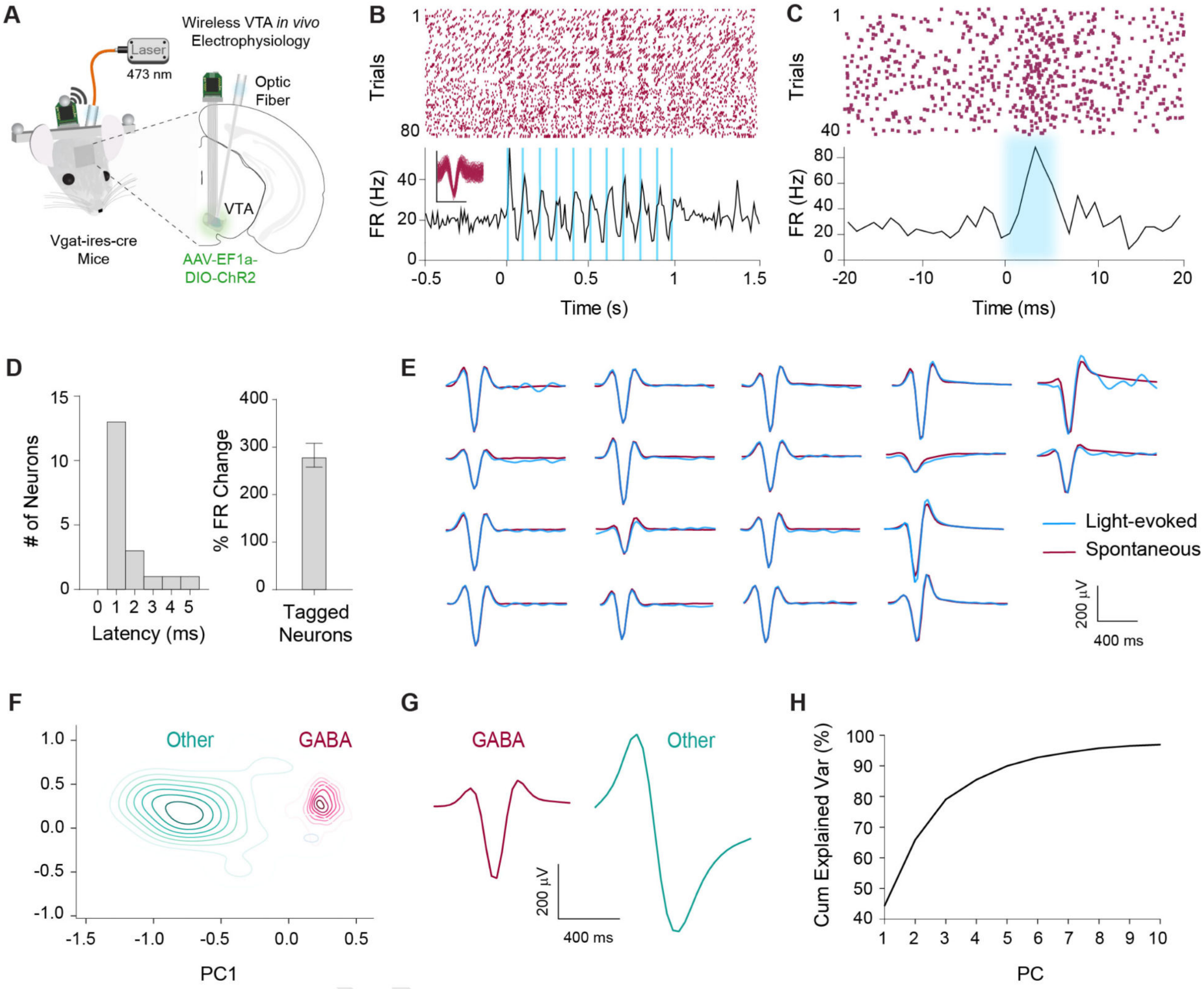

Figure 1. Optogenetic identification of VTA$^{\text{Vgat+}}$ neurons.

(A) Schematic illustration of optrode in the VTA for simultaneous optogenetic excitation and recording of *VGAT+* neurons in *Vgat-ires-Cre* mice ($n = 6$).

(B) Representative example of an optically tagged VTA$^{\text{Vgat+}}$ neuron using 10 Hz stimulation.

(C) Another representative neuron showing very short latency in response to light stimulation.

(D) *Left*: All tagged GABAergic neurons had a latency of < 6 ms ($n = 18$). *Right*: Optically tagged GABAergic neurons displayed a significant increase in firing rate in response to light stimulation compared to baseline ($p < .0001$).

(E) Fidelity analysis demonstrating similarity of waveforms between spontaneous (maroon) and light-evoked (blue) waveforms.

(F) Contour plot of the first two principal components out of 10 within an unsupervised clustering of neuronal waveforms. *Post hoc* analysis revealed all optically tagged VTA$^{\text{Vgat+}}$

neurons fell within one cluster. The remaining neurons that fell within the same cluster were classified as putative GABAergic neurons.

(G) Average waveforms for cells classified as GABAergic ($n = 421$) or other ($n = 58$).

(H) Cumulative explained variance for each principal component. Ten principal components accounted for over 95% of the variance within the neuronal waveforms. See also Figure S7.

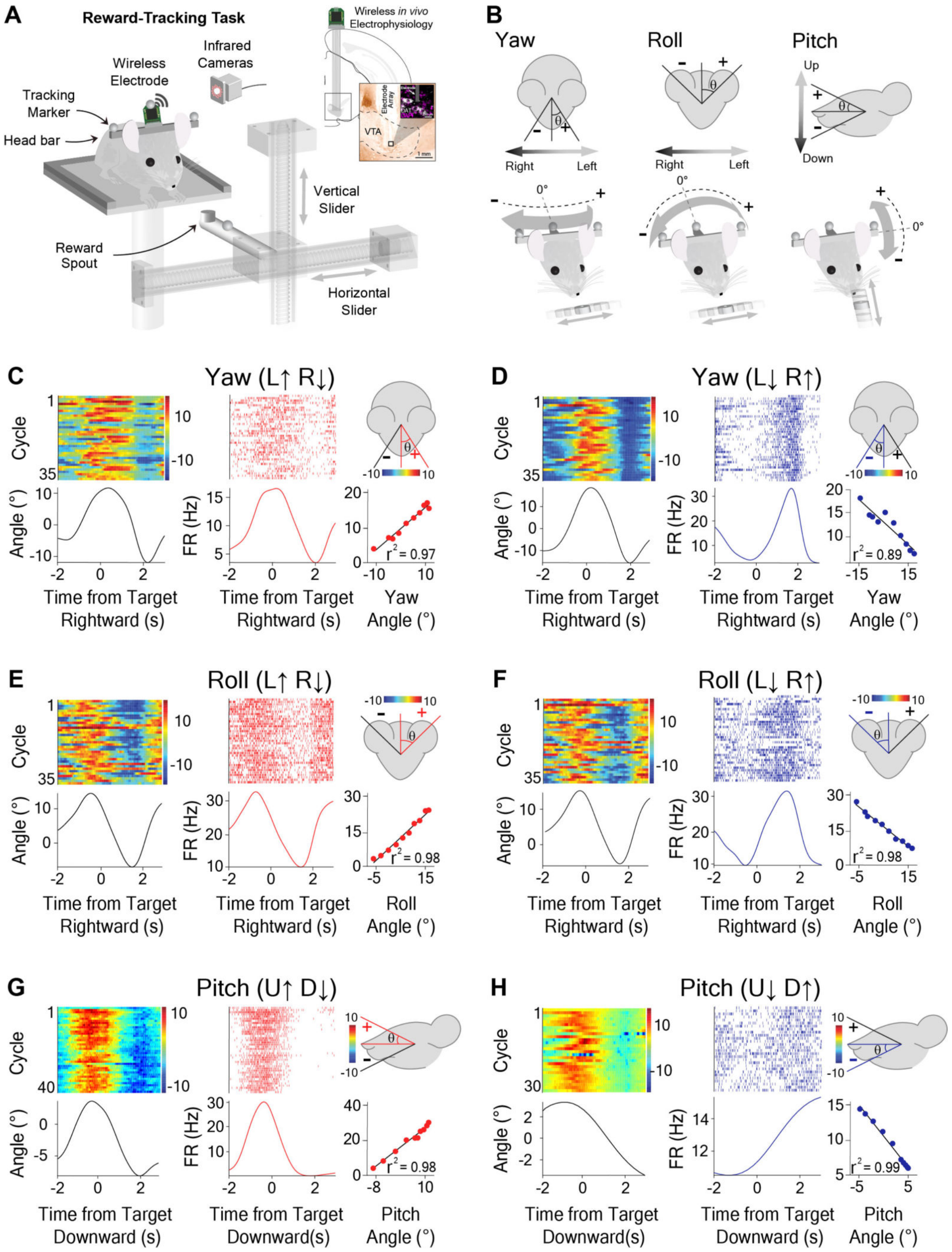

Figure 2. Opponent encoding of yaw, roll, and pitch angles by VTA GABAergic neurons.

(A) Schematic of reward-tracking task during VTA wireless *in vivo* electrophysiology. Mice (*Wild-Type* mice, *n* = 20) tracked a moving spout in the horizontal and vertical directions to receive a reward (diluted condensed milk). Infrared cameras captured kinematic data from markers on the head of the animal with respect to reward target. Inset shows schematic of electrode placement into the VTA and representative histological section in the vicinity of DAT-positive cells.

(B) Schematic representation and sign conventions for yaw (*left*), roll (*middle*), and pitch (*right*) rotational kinematics. Arrows show direction of head movement around each axis. Zero angle is when the animal has his head straight forward.

(C-H) Individual neurons represent direction-specific angles along orthogonal axes of rotation. Peri-event heat maps of head angle (*left*), peri-event raster plots of VTA neural activity (*middle)* with respect to reward target, and a correlation graph (*right bottom*) with a schematic illustration demonstrating head angle direction for which the firing rate increases (*right top*).

(C) Yaw angle and Yaw (L↑ R↓) neuron during horizontal tracking (*Pearson Correlation* (*PC*), $r^2 = 0.97$, $p < 0.0001$).

(D) Yaw angle and Yaw (L↓ R↑) neuron during horizontal tracking (*PC,* $r^2 = 0.89$, $p < 0.0001$).

(E) Roll angle and Roll (L↑ R↓) neuron during horizontal tracking (*PC,* $r^2 = 0.98$, $p < 0.0001$).

(F) Roll angle and Roll (L↓ R↑) neuron during horizontal tracking (*PC,* $r^2 = 0.98$, $p < 0.0001$).

(G) Pitch angle and Pitch (U↑ D↓) neuron during vertical tracking (*PC,* $r^2 = 0.98$, $p < 0.0001$).

(H) Pitch angle and Pitch (U↓ D↑) neuron during vertical tracking (*PC,* $r^2 = 0.99$, $p < 0.0001$). See also Figures S1–S3 and S7, Videos S1–S3.

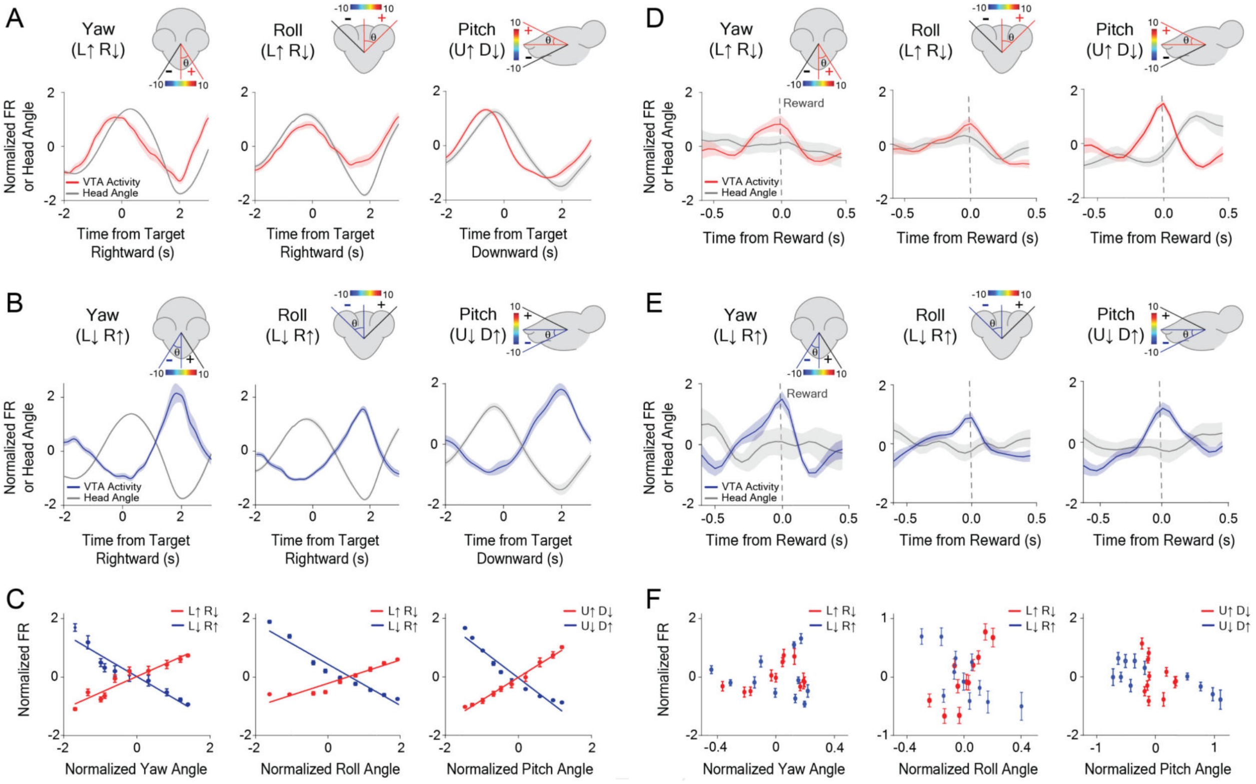

Figure 3. VTA GABAergic ensembles represent yaw, roll, and pitch, but these representations degrade at the time of reward.

(A-C) Population activity precisely represents orthogonal angles of head rotation.

(A) Neuronal population for Yaw (L↑ R↓, increase firing with leftward tilt and decrease firing with rightward tilt) neurons (*left*, $n = 16$), Roll (L↑ R↓) neurons (*middle*, $n = 28$), and Pitch (U↑ D↓) neurons (*right*, $n = 16$) during reward tracking. Traces and error bars represent the Mean ± SEM.

(B) Opponent neuronal populations for Yaw (L↓ R↑) neurons (*left*, $n = 10$), Roll (L↓ R↑) neurons (*middle*, $n = 34$), and Pitch (U↓ D↑) neurons (*right*, $n = 13$) during reward tracking.

(C) Population average showing correlation between head angle and VTA neuronal firing rate while tracking reward: Yaw angle (*left*) (Yaw (L↑ R↓): *PC*, $r^2 = 0.91$, $p < .0001$, $n = 16$; Yaw (L↓ R↑): *PC*, $r^2 = 0.92$, $p < 0.0001$, $n = 10$). Roll Angle (*middle*) (Roll (L↑ R↓): *PC*, $r^2 = 0.92$, $p < 0.0001$, $n = 28$; Roll (L↓ R↑): *PC*, $r^2 = 0.94$, $p < 0.0001$, $n = 34$). Pitch Angle (*right*) (Pitch (U↑ D↓): *PC*, $r^2 = 0.99$, $p < 0.0001$, $n = 16$; Pitch (U↓ D↑): *PC*, $r^2 = 0.94$, $p < 0.0001$, $n = 13$).

(D-F) Degradation of neural coding for head angle at the time of reward consumption.

(D) Neural population for Yaw (L↑ R↓) neurons (*left*, $n = 16$), Roll (L↑ R↓) neurons (*middle*, $n = 28$), and Pitch (U↑ D↓) neurons (*right*, $n = 16$) at the time of reward.

(E) Neural population for Yaw (L↓ R↑) neurons (*left*, $n = 10$), Roll (L↓ R↑) neurons (*middle*, $n = 34$), and Pitch (U↓ D↑) neurons (*right*, $n = 13$) at the time of reward.

(F) Population average showing correlation between head angle and firing rate during reward consumption: Yaw angle (*left*) (Yaw (L↑ R↓): *PC*, $r^2 = 0.18$, $p > 0.05$ $n = 16$; Yaw (L↓ R↑): *PC*, $r^2 = 0.005$, $p > 0.05$, $n = 10$). Roll Angle (*middle*) (Roll (L↑ R↓): *PC*, $r^2 = 0.65$, $p = 0.003$, $n = 28$; Roll (L↓ R↑): *PC*, $r^2 = 0.53$, $p = 0.01$, $n = 34$). Pitch Angle (*right*)

(Pitch (U↑ D↓): *PC*, $r^2 = 0.09$, $p > 0.05$, $n = 16$; Pitch (U↓ D↑): *PC*, $r^2 = 0.56$, $p = 0.01$, $n = 13$). Traces and error bars represent the Mean ± SEM.

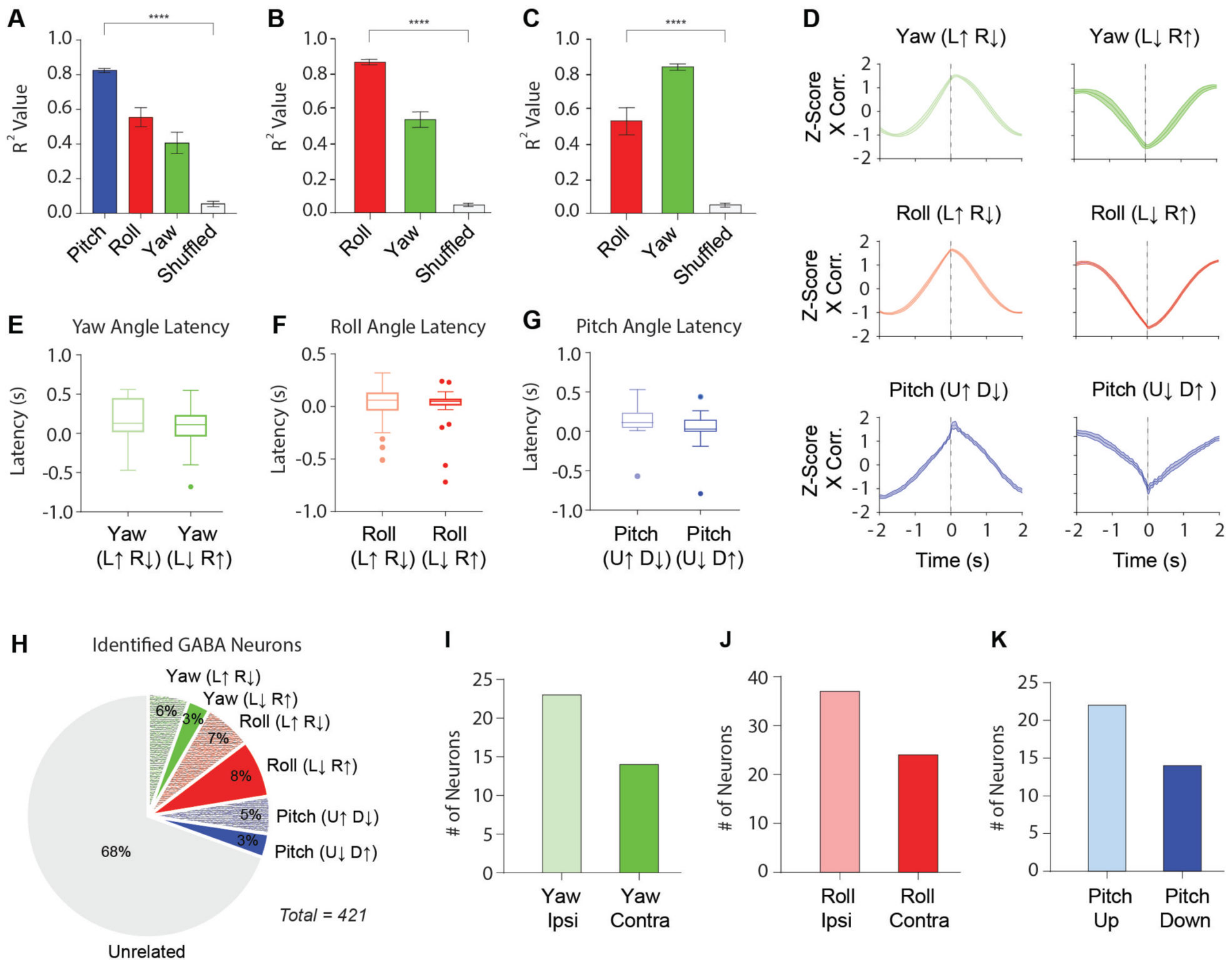

Figure 4. Summary of classified VTA GABAergic neurons.

(A) Average r^2 values for yaw, roll, and pitch, as well as shuffled data from a Pearson Correlation (*PC)* analysis for neurons classified as pitch. (Pitch: $r^2 = 0.83 \pm 0.01$; Roll: $r^2 = 0.56 \pm 0.03$; Yaw: $r^2 = 0.41 \pm 0.05$; Mean ± SEM). Correlation with pitch angle is significantly higher than correlation with roll and yaw angles (One-way ANOVA: $F_{(3,134)} = 62.64$, $p < 0.0001$; *p* values were corrected with Dunnett's multiple comparison test. **** $p < 0.0001$).

(B-C) Because yaw and roll co-varied during horizontal tracking and had similar r^2 values when compared to the pitch population, we directly compared r^2 values between roll and yaw angle along with shuffled data for neurons classified as yaw or roll angle neurons.

(B) There is a significant difference between the r^2 values of yaw and roll angle for neurons categorized as roll neurons (One-way ANOVA, $F_{(2,195)} = 60.31$, $p < 0.0001$, Roll: $r^2 = 0.87 \pm 0.01$; Yaw: $r^2 = 0.54 \pm 0.03$; Mean ± SEM).

(C) There is also a significant difference between the r^2 values of yaw and roll angle for neurons categorized as yaw neurons (One-way ANOVA, $F_{(2,90)} = 37.36$, $p < 0.0001$, Yaw: $r^2 = 0.83 \pm 0.01$; Roll: $r^2 = 0.54 \pm 0.05$; Mean ± SEM).

(D) Normalized cross-correlations for yaw neurons (*top*), roll neurons (*middle*), and pitch neurons (*bottom*). Latency between neural activity and behavior were determined from cross-correlation analysis.

(E) Latency between neural activity and yaw angle for both Yaw (L↑ R↓; $\bar{x}$ = 180 ± 0.05 ms) and Yaw (L↓ R↑; $\bar{x}$ = 52 ± 0.09 ms; Mean ± SEM) neurons.

(F) Latency between neural activity and roll angle for both Roll (L↑ R↓; $\bar{x}$ = 60 ± 0.03 ms) and Roll (L↓ R↑; ($\bar{x}$ = 50 ± 0.03 ms; Mean ± SEM) neurons.

(G) Latency between neural activity and pitch angle for both Pitch (U↑ D↓; $\bar{x}$ = 130 ± 0.04 ms) and Pitch (U↓ D↑; $\bar{x}$ = 20 ± 0.07 ms; Mean ± SEM) neurons.

(H) Proportion of head angle neurons among all classified VTA GABAergic neurons.

(I) Number of yaw angle neurons that increase their firing rate in the ipsiversive direction (n = 23) or contraversive direction (n = 14) in relation to the recording hemisphere.

(J) Number of roll angle neurons that increase their firing rate in the ipsiversive direction (n = 37) or contraversive direction (n = 24) in relation to the recording hemisphere.

(K) Number of pitch angle neurons that increase their firing rate in the upward direction (n = 22) or downward direction (n = 14). See also Figure S4 and Videos S4 and S5.

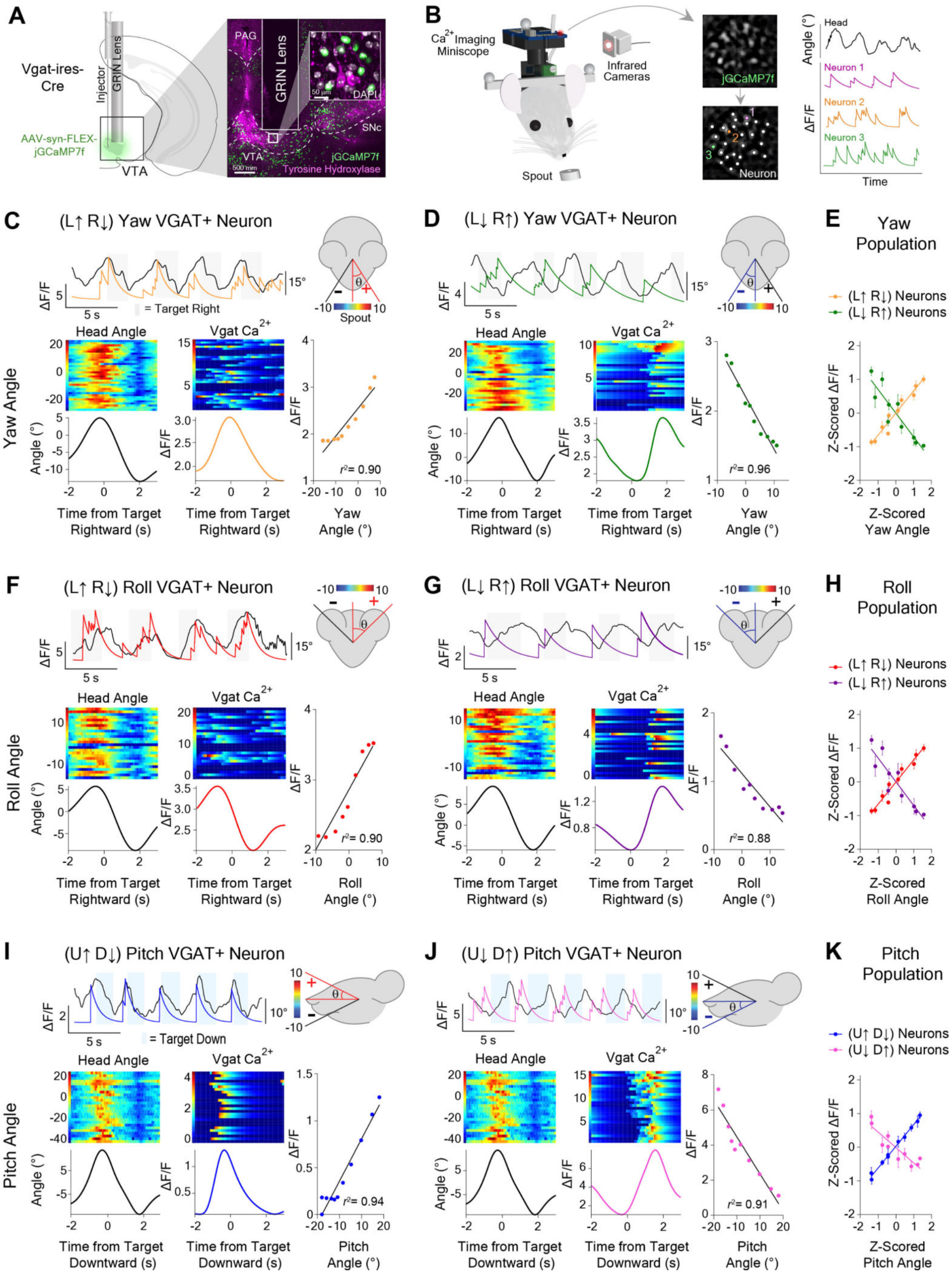

Figure 5. Orthogonal head angle representations demonstrated with *in vivo* calcium imaging of VTA^{Vgat+} neurons.

(A) GRIN lens implantation over AAV-hSyn-GCaMP7f infected GABAergic cells in the VTA of *Vgat-ires-Cre* mice (*n* = 7) for chronic *in vivo* recordings of calcium fluctuations. Representative coronal section through the midbrain shows calcium indicator (jGCaMP7f) expression near tyrosine hydroxylase neurons in the VTA.

(B) Schematic illustration of 1-photon miniscope attached to mouse head for calcium imaging during reward tracking behavior (*left*). Extracted changes in fluorescent intensity of $\text{VTA}^{\text{Vgat+}}$ neurons concomitant with rotational head kinematics (*right*).

(C-J) $\text{VTA}^{\text{Vgat+}}$ neurons represent head angles about three orthogonal axes of rotation. Raw calcium transients and angle behavior over 20s (*top*). Black traces represents head angle, colored traces represent deconvolved calcium transients. Peri-event heat maps of head angle (*left*) and calcium activity (*middle*). Correlation between neural activity and angle (*right*).

(C) Yaw (L↑ R↓) neuron (*PC*, $r^2 = 0.90$, $p < 0.0001$).

(D) Yaw (L↓ R↑) neuron (*PC*, $r^2 = 0.96$, $p < 0.0001$).

(E) Correlation for Yaw angle population (Yaw (L↑ R↓): *PC,* $r^2 = 0.95$, $p < 0.0001$, $n = 18$; Yaw (L↓ R↑): *PC,* $r^2 = 0.83$, $p = 0.0002$, $n = 14$).

(F) Roll (L↑ R↓) neuron (*PC*, $r^2 = 0.90$, $p < 0.0001$)

(G) Roll (L↓ R↑) neuron (*PC*, $r^2 = 0.88$, $p < 0.0001$).

(H) Correlation analyses for Roll angle population (Roll (L↑ R↓): *PC,* $r^2 = 0.94$, $p < 0.0001$, $n = 16$; Roll (L↓ R↑): *PC,* $r^2 = 0.65$, $p = 0.005$, $n = 14$).

(I) Pitch (U↑ D↓) neuron (*PC*, $r^2 = 0.94$, $p < .0001$).

(J) Pitch (U↓ D↑) neuron (*LR*, $r^2 = 0.91$, $p < 0.0001$).

(K) Correlation for Pitch angle population (Pitch (U↑ D↓): *PC,* $r^2 = 0.99$, $p < 0.0001$, $n = 15$; Pitch (U↓ D↑): *PC,* $r^2 = 0.82$, $p = 0.0003$, $n = 12$). Also see Figures S5 and S7.

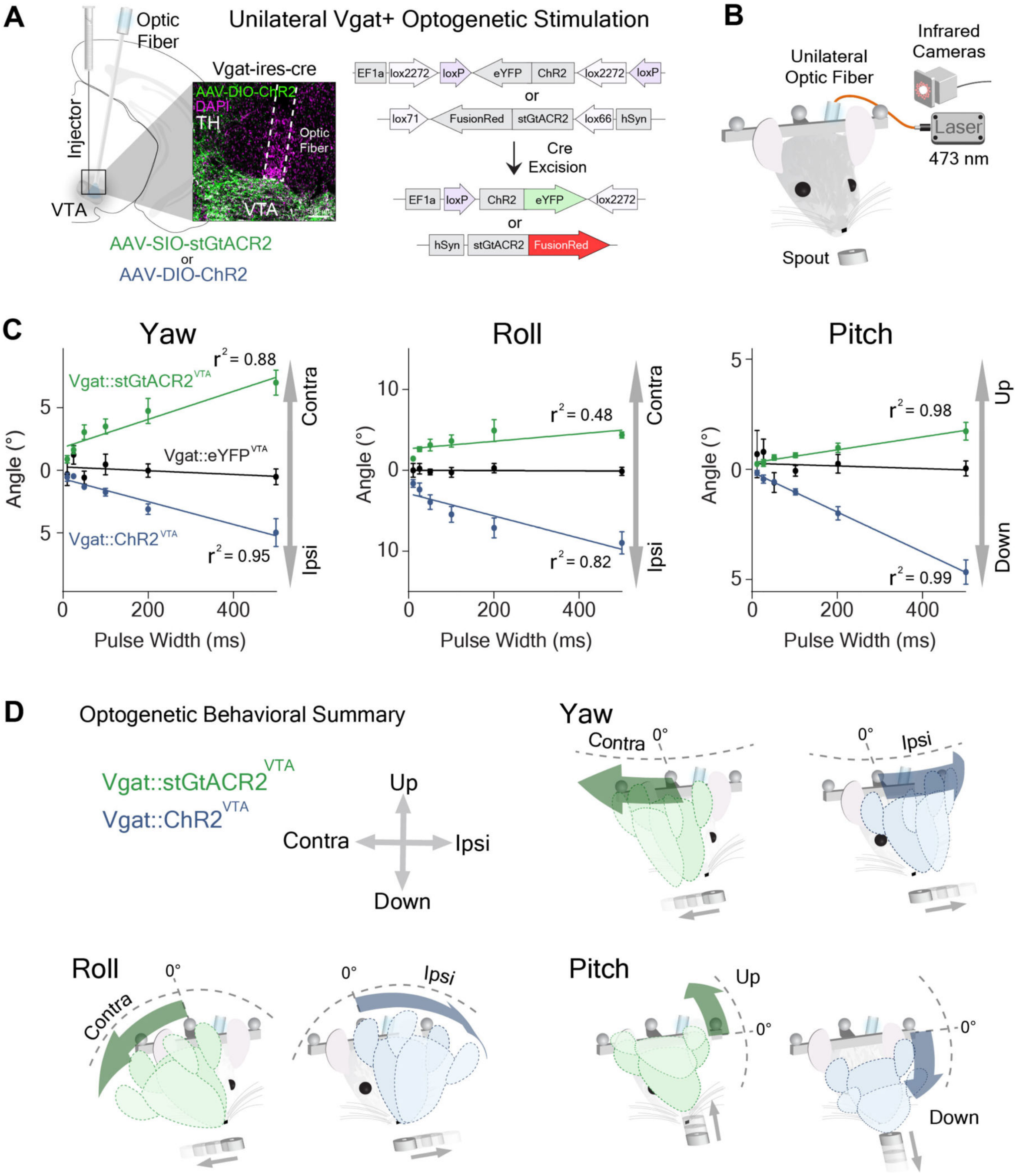

Figure 6. Optogenetic excitation and inhibition produce opposite deviations in head angles.

(A) Unilateral stimulation of VTA^{Vgat+} neurons. AAV-DIO-ChR2 or AAV-SIO-StGtACR2 was injected into the VTA of *Vgat-ires-Cre* mice. Inset shows ChR2 in the vicinity of TH-positive cells. Note glial scarring caused by optic fiber above VTA.

(B) Schematic of unilateral optogenetic stimulation during reward tracking.

(C) Optogenetic relationship between pulse width and deviation of pitch (*left*), roll (*middle*) and yaw (*right*) angles (*two-way RM* ANOVA, Yaw Angle, Main effect of Group, $F_{(2,17)} = 91.93$, $p < 0.0001$; Roll Angle, Main effect of Group, $F_{(2,167)} = 72.04$, $p < 0.0001$; Pitch

Angle, Main effect of Group, $F_{(2,17)} = 35.63$, $p < 0.0001$, ChR2: $n = 6$; StGtaCR2: $n = 6$; control: $n = 7$).

(D) Schematic illustration of the effects of stimulation on yaw, roll, and pitch. Optogenetic excitation produces ipsiversive and downward deviations of head angles, while inhibition produces contraversive and upward deviations of head angles. Also see Figures S6–S7, Videos S4 and S5.

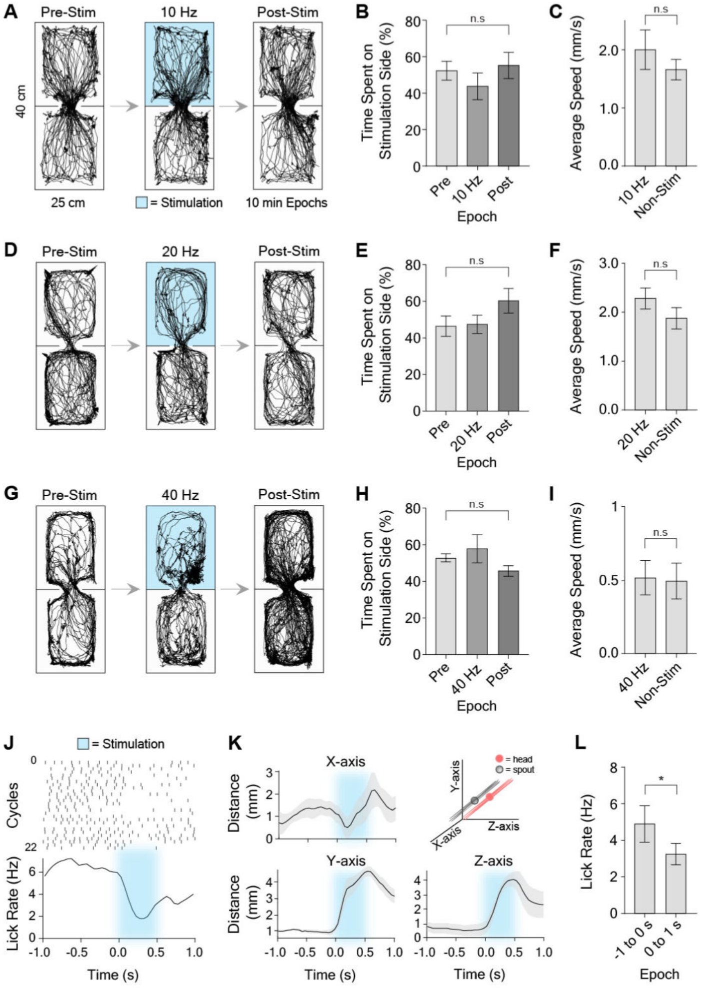

Figure 7. VTA stimulation has no effect in real-time conditioned place preference, but reduces reward consumption in reward-tracking task.

(A) Raw traces during real-time conditioned place preference assay using 10 Hz stimulation (10 ms pulse width). Mice were placed into a chamber for a total of 30 minutes across three epochs (pre-stimulation, stimulation, post-stimulation epochs; 10 min per epoch). During the stimulation epoch, 10 Hz unilateral stimulation was delivered when the animal was in the top half of the chamber.

(B) There was no significant difference between the time spent on the 10 Hz stimulation (10 ms pulses) side versus the pre- and post-stimulation epochs (RM one-way ANOVA, $F_{(2,21)} = 3.99$, $p = 0.01$, $n = 8$. *Post-hoc* analysis that corrected for multiple comparisons, however, revealed no significant differences between groups, $p > 0.05$).

(C) Average speed during 10Hz stimulation epoch on the stimulation half of the chamber was not significantly different than the non-stimulation half (paired t-test, $t_{(7)} = 0.89$, $p > 0.05$, $n = 8$).

(D) Raw traces during real time-CPP during 20 Hz stimulation.

(E) There was no significant difference between the time spent on the 20 Hz stimulation (10 ms pulses) half of the chamber versus the pre- and post-stimulation epochs; RM one-way

ANOVA, $F_{(2,21)} = 3.48$, $p = 0.02$, $n = 8$. *Post-hoc* analysis that corrected for multiple comparisons revealed no significant differences between groups, $p > 0.05$).

(F) Average speed during 20 Hz stimulation epoch on the stimulation side of the chamber was not significantly different than the non-stimulation side (paired t-test, $t_{(7)} = 0.09$, $p > 0.05$, $n = 8$).

(G) Raw traces during real time-CPP during 40 Hz stimulation.

(H) There was no significant difference between the time spent on the 40 Hz stimulation (10 ms pulses) half of the chamber versus the pre- and post-stimulation epochs; RM one-way ANOVA, $F_{(2,15)} = 0.38$, $p > 0.05$, $n = 6$).

(I) Average speed during 40 Hz stimulation epoch on the stimulation side of the chamber was not significantly different than the non-stimulation side (paired t-test, $t_{(5)} = 0.35$, $p > 0.05$, $n = 6$).

(J-L) Licking-related activity during reward tracking task.

(J) Representative licking raster during 500 ms of optogenetic excitation. Top panel is a peri-event raster plot, where each dash represents a lick, and each row represents one cycle. Bottom panel is average lick rate plot. Excitation produced a reduction in licking during and immediately after licking.

(K) Population graphs showing increased distance to the target due to stimulation for all three axes ($n = 6$).

(L) Average lick rate was significantly reduced during and immediately after stimulation compared to before stimulation (paired t-test, $t_{(5)} = 3.20$, $p = 0.02$, $n = 6$).

Key Resources Table

REAGENT or RESOURCE	SOURCE	IDENTIFIER
Antibodies		
Goat polyclonal anti-Rabbit Alexa Fluor 488	Abcam	Cat# ab150077; RRID: AB_2630356
Goat polyclonal anti-Rabbit Alexa Fluor 594	Abcam	Cat# ab150080; RRID: AB_2650602
Rabbit polyclonal anti-Dopamine Transporter	Abcam	Cat# ab111468; RRID: AB_11155293
Rabbit polyclonal anti-Tyrosine Hydroxylase	Millipore	Cat# 657012; RRID: AB_566341
Rabbit polyclonal anti-Vesicular GABA Transporter	Millipore	Cat# AB5062P; RRID: AB_2301998
Bacterial and Virus Strains		
rAAV5-EF1α-DIO-eYFP	Duke Vector Core	N/A
rAAV5-EF1α-DIO-hChR2(H134R)-eYFP	Duke Vector Core	N/A
pGP-AAV1-syn-jGCaMP7f-WPRE	Addgene	Cat# 10448-AAV1
AAV1-hSyn-SIO-stGtACR2-FusionRed	Addgene	Cat# 105677-AAV1
Experimental Models: Organisms/Strains		
Mouse: Vgat-ires-Cre: $1^{\text{tm2(cre)Lowl}}$/J	Jackson Laboratory	Mouse Strain: 016962
Mouse: C57BL/6J	Jackson Laboratory	Mouse Strain: 000664
Oligonucleotides		
Primers for Vgat-ires-Cre (F: GGTCGATGCAACGAGTGATGAGG) (R: GCCAGATTACGTATATCCTGGCAG)	Integrated DNA Technologies	N/A
Software and Algorithms		
MATLAB 2016b	MathWorks	https://www.mathworks.com/products/new_products/release2015b.html
Python 2.7	Anaconda	https://www.anaconda.com/download/?lang=en-us
Bonsai	Open Ephys	http://www.open-ephys.org/bonsai/
Offline Sorter 3.0	Plexon	https://plexon.com/products/offline-sorter/
NeuroExplorer 4.0	Nex Technologies	http://www.neuroexplorer.com/downloadspage/
Cortex 5.0	MotionAnalysis	http://ftp.motionanalysis.com/html/industrial/cortex.html
GraphPad Prism 8	GraphPad	https://www.graphpad.com/scientific-software/prism/
Other		
LED Driver	Thorlabs	LEDD1B
DAPI Fluoromount-G	Southern Biotech	Cat# 0100-20